Journal of Biomechanics 84 (2019) 153–160

Contents lists available at ScienceDirect

Journal of Biomechanics

journal homepage: www.elsevier.com/locate/jbiomech
www.JBiomech.com

A lower extremity model for muscle-driven simulation of activity using explicit finite element modeling

Donald R. Hume *, Alessandro Navacchia, Paul J. Rullkoetter, Kevin B. Shelburne

University of Denver, Center for Orthopaedic Biomechanics, Denver, CO, United States

ARTICLE INFO

Article history:
Accepted 22 December 2018

Keywords:
Musculoskeletal modeling
Finite element
Squatting
Gait
Knee
Muscle

ABSTRACT

A key strength of computational modeling is that it can provide estimates of muscle, ligament, and joint loads, stresses, and strains through non-invasive means. However, simulations that can predict the forces in the muscles during activity while maintaining sufficient complexity to realistically represent the muscles and joint structures can be computationally challenging. For this reason, the current state of the art is to apply separate rigid-body dynamic and finite-element (FE) analyses in series. However, the use of two or more disconnected models often fails to capture key interactions between the joint-level and whole-body scales. Single framework MSFE models have the potential to overcome the limitations associated with disconnected models in series. The objectives of the current study were to create a multi-scale FE model of the human lower extremity that combines optimization, dynamic muscle modeling, and structural FE analysis in a single framework and to apply this framework to evaluate the mechanics of healthy knee specimens during two activities. Two subject-specific FE models (Model 1, Model 2) of the lower extremity were developed in ABAQUS/Explicit including detailed representations of the muscles. Muscle forces, knee joint loading, and articular contact were calculated for two activities using an inverse dynamics approach and static optimization. Quadriceps muscle forces peaked at the onset of chair rise (2174 N, 1962 N) and in early stance phase (510 N, 525 N), while gait saw peak forces in the hamstrings (851 N, 868 N) in midstance. Joint forces were similar in magnitude to available telemetric patient data. This study demonstrates the feasibility of detailed quasi-static, muscle-driven simulations in an FE framework.

1. Introduction

Musculoskeletal modeling allows researchers to gain insight into the interaction of muscle and joint mechanics that cannot practically be measured in the laboratory (Fernandez and Hunter, 2005; Hume et al., 2018; Shelburne et al., 2005). A key challenge of the computational approach is determining the forces in the muscles during activity while maintaining sufficient complexity to realistically represent the tissues. Muscle forces contribute to joint load and have a strong influence on joint mechanics (Lenhart et al., 2015), which in turn partially determine muscle length, line-of-action, and moment arm (Fiorentino, 2013; Hume et al., 2018; Navacchia et al., 2017). This interaction is an important relationship that influences the biomechanics of the musculoskeletal system and can only be described in a model that incorporates both joint deformation and muscle mechanics (Hume et al., 2018; Shelburne and Pandy, 2002). Treatments that change or seek to restore healthy joint mechanics are rarely evaluated through a lens that includes the interaction of joint kinematics with muscle function.

The current state of the art is to utilize a rigid-body musculoskeletal model to calculate a muscle loading condition that is then applied to a detailed joint-level FE model (Adouni and Shirazi-Adl, 2014a; Navacchia et al., 2016b). Rigid body dynamic analyses (e.g. OpenSim, AnyBody) represent whole-body motions and may include large numbers of muscles. When used in conjunction with optimization, they can be used to predict forces in individual muscles required to perform an activity (Anderson and Pandy, 2001a; Besier et al., 2009; Smith et al., 2015). These analyses are computationally efficient, but have limited joint-level fidelity because the knee joint is often represented as a hinge (Anderson and Pandy, 2001a) or with secondary degrees of freedom (DOF) prescribed as a function of flexion angle (Arnold and Delp, 2011; Delp et al., 2007), and muscle geometry is limited to wrapping of line segments over geometric primitives. The output of rigid body simulations can be applied to a detailed FE model

* Corresponding author at: Dept. of Mechanical and Materials Engineering, The University of Denver, 2155 East Wesley, Denver, CO 80208, United States.
E-mail address: don.hume@du.edu (D.R. Hume).

https://doi.org/10.1016/j.jbiomech.2018.12.040
0021-9290/

focused on the joint of interest. FE analysis allows for representation of structures such as joints and ligaments in sufficient detail for accurate solutions of the internal stresses and strains including complex contact conditions and material representations such as anisotropic hyperelastic behavior (Fitzpatrick et al., 2010), with the tradeoff of longer computational times. In a detailed representation of the joint, muscle forces drive changes in joint mechanics through DOFs which would otherwise remain unaffected in a rigid body modeling application.

Single framework MSFE models have the potential to overcome the limitations associated with using disconnected models in series by combining muscle force estimation and deformable FE analysis. For example, it has been shown that knee contact forces contribute substantially to the resultant joint torques (Walter et al., 2015). These contributions would not be included in the inverse dynamics solutions of rigid body analyses ultimately affecting the muscle force predictions. Even so, prior studies which performed muscle force optimization in an FE framework were often limited in complexity to avoid lengthy computational time (Adouni et al., 2012; Halloran et al., 2010, 2009; Lin et al., 2010). Notably, Lin et al. (2010) and Adouni et al. (2012) used an FE model to obtain simultaneous muscle force and joint contact solutions for gait. However, these researchers modeled the muscles as ideal actuators, setting aside the elasticity of tendon and the force-length properties of muscle. As computational power continues to improve and becomes less limiting, effective parallelization of static optimization routines will become increasingly viable for simulations in an FE framework.

The objectives of this study were (1) to create a multi-scale musculoskeletal finite element (MSFE) model of the human lower extremity that combined muscle modeling and deformable FE analysis into a single model, (2) and to test whether static optimization can be practically applied to achieve simulation of human activity. Simultaneous analyses of muscle and joint function during physical activity can improve assessment of lower-limb function and help to inform surgical and clinical practice.

2. Methods

2.1. Human experiments

Laboratory measurements were collected from 2 healthy subjects during chair rise (Subject 1, age 60 yr, 174 cm, 74.8 kg) and gait (Subject 2, age 59 yr, 177.2 cm, 74.4 kg). The subjects provided informed consent to participate in a University of Denver IRB approved study. Each subject was screened for history of orthopedic injury to the lower extremity joints. Kinematic, force-plate, and EMG data were collected for a battery of activities testing function during activities of daily living (Kefala et al., 2017). Two subjects and two activities were chosen to test the robustness of the proposed methodology. Ground reaction forces were measured with strain-gauged force platforms (Bertec Corp, Columbus, OH) embedded in the laboratory floor. Active EMG surface electrodes (Noraxon USA, Scottsdale, AZ) recorded activity of six dominant lower extremity muscles. Raw EMG data were rectified, filtered, and normalized to maximum isometric contractions, and used for validating the muscle activations predicted in the computer simulations. The positions of passive retro-reflective markers mounted on the body were measured using an eight-camera motion-capture system (Vicon Motion Systems Inc., Centennial, CO). Joint angles were calculated from the marker positions using a rigid body modeling software package (OpenSim, Stanford, CA). A high-speed stereo radiography (HSSR) system was used in conjunction with motion capture to calculate six degree of freedom (DOF) kinematics for the dominant knee during each task (Kefala et al., 2017). Lower limb kinematics and ground reaction forces were used as input to the musculoskeletal simulations of gait and chair rise.

2.2. Musculoskeletal model

Two MSFE models of the lower limb including knee models of healthy specimens were created for dynamic analyses in ABAQUS/Explicit (SIMULIA, Providence, RI) (Fig. 1). Two distinct knee models with specimen-specific articular geometry and calibrated laxity response were used to test the robustness of single-framework FE to changes in joint mechanics. The formulation for the model of the knees has been discussed previously (Ali et al., 2017, 2016; Harris et al., 2016; Hume et al., 2018) but will be summarized below. The models included specimen-specific bone and cartilage geometry which were segmented from CT and MRI, respectively. Contact was modeled with a pressure-overclosure relationship, based on elastic foundation theory, previously verified to accurately mimic deformable contact (Fitzpatrick et al., 2010). The model included a 1 DOF hinge-joint at the ankle, a 3 DOF ball-joint at the hip, and 6 DOF joints representing the tibiofemoral (TF) and patellofemoral (PF) joints.

TF and PF ligaments were calibrated to specimen specific laxity and flexion-extension tests (Ali et al., 2016; Harris et al., 2016). Seven ligamentous structures crossing the tibiofemoral joint were represented including the anterior and posterior cruciate ligaments (ACL, PCL), medial and lateral collateral ligaments (MCL, LCL), popliteofibular ligament (PFL), anterolateral ligament (ALS), and both medial and lateral representations of the posterior capsule (PCAP) (Harris et al., 2016). Ligaments were modeled as bundles of point-to-point non-linear springs and were calibrated to the joint laxity envelope of the same specimens whose geometry was used to build the knees (“S1” and “S2” in Harris et al.). Patellar and quadriceps tendon were modeled as 2D reinforced membrane elements permitted to wrap over cartilage and bone (Baldwin et al., 2009).

Twenty muscles spanning the hip, knee, and ankle were represented as 3-element Hill-type muscles. The muscles represented in the model were soleus, gastrocnemius (medialis and lateralis), tibialis anterior, vastus medialis (3 musculotendon units), vastus intermedius, vastus lateralis (2 units), rectus femoris, semimembranosus, semitendinosus, biceps femoris short and long head, gluteus maximus (3 units), iliacus, and psoas. Insertion and origin were derived initially from anatomical landmarks as reported by Delp et al. (2007). Muscle geometries were calibrated such that passive moment arms matched values reported from *in vitro* experiments (Buford et al., 1997). Hill-type muscle model parameters were calibrated to match mean isometric flexion and extension torque curves recorded from healthy subjects (Hume et al., 2018).

2.3. Calculation of muscle forces in chair rise and gait

Muscle activations and forces, and joint loads and contact forces were calculated for the chair rise activity and during the stance phase of gait in a finite element framework. Using a quasi-static inverse dynamics approach, muscle forces were estimated using static optimization at six body positions throughout the chair rise and seven body positions during gait. Static optimization was chosen due to its widespread use in solving the muscle redundancy problem common in musculoskeletal modeling (Crowninshield and Brand, 1981). For activities that do not involve rapid movement, a quasi-static analysis is reasonable because inertial forces contribute little to tissue loading (Anderson and Pandy, 2003). The inputs to the static optimization were the joint angles of the hip, knee, and ankle joints, and the ground reaction forces and centers of pressure applied relative to the foot center of mass (COM).

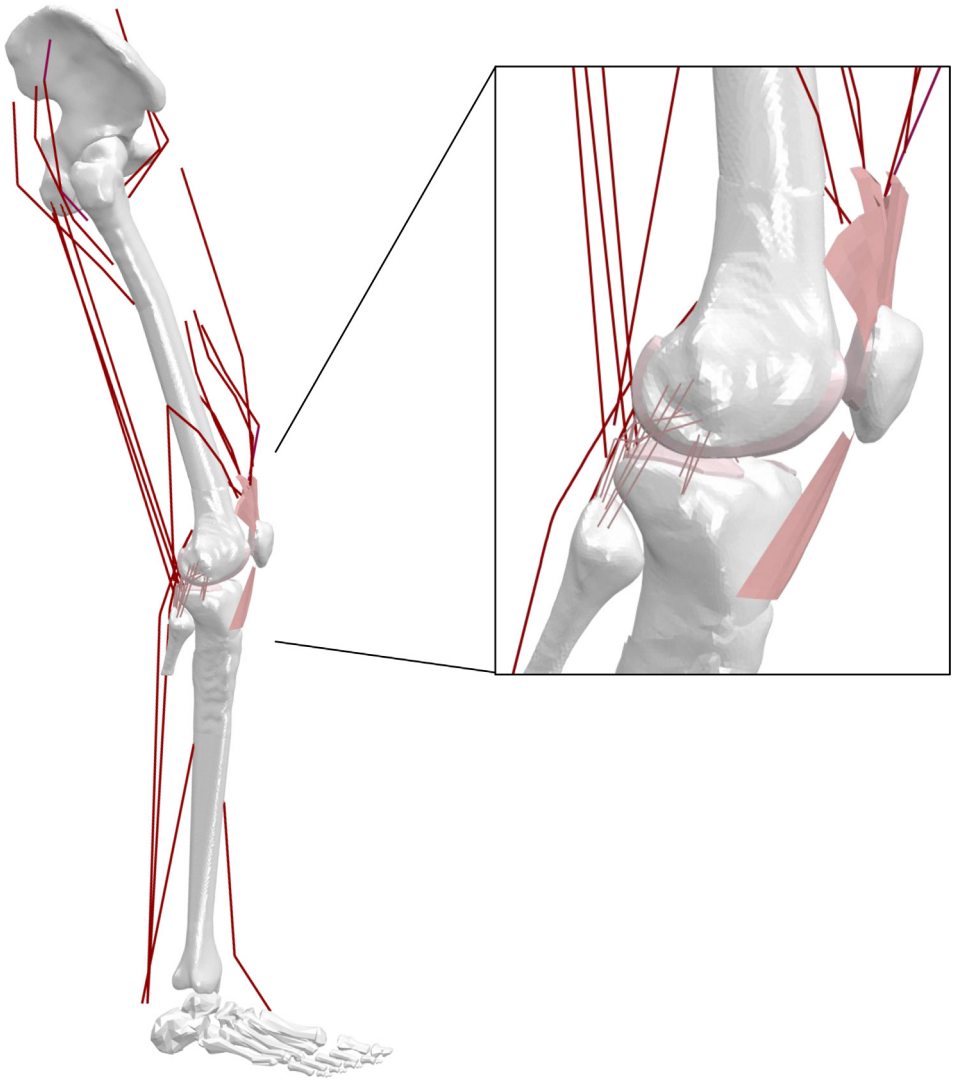

Fig. 1. The lower limb musculoskeletal finite element model with two calibrated specimen specific knees (M1 pictured). The knees included TF and PF soft tissue structures whose response was calibrated to *in vitro* experiments (Ali et al., 2016; Harris et al., 2016). The model includes 15 unique muscles comprised of 20 musculotendon fibers which span the lower limb previously calibrated to match mean healthy isometric knee flexion-extension torque results (Hume et al., 2018).

In the ABAQUS/Explicit simulation, the kinematics of the hip, knee, and ankle were enforced by residual torques applied at the joints to maintain the required position. The remaining DOF of the tibiofemoral and patellofemoral joints were unconstrained and determined based on the interaction between tibiofemoral and patellofemoral contact force, muscle force, and ligament restraint. The variables in the optimization design vector were the activation levels of the muscles. An initial guess for these values was obtained from the normalized subject EMG. The optimization found the muscle activations that reduced the residual flexion-extension torques to less than 1 Nm at the hip, knee, and ankle and minimized the sum of the cube of muscle stress (Crowninshield and Brand, 1981).

Static optimization was implemented in MATLAB (Mathworks, Natick, MA) using the Nelder-Mead Simplex method, which combined ABAQUS/Explicit concurrent simulations of each activity's time points with muscle force calculations using subroutines written in MATLAB and Python. Separate optimizations were performed simultaneously at each of 13 time points representing two activities using a custom computational framework that managed parallel process control. During the optimization, each FE simulation used the current design vector of muscle activations coupled with the previous kinematic pose and corresponding muscle geometry to estimate muscle forces for each time point. Each optimization concluded when the improvements on the cost function became less than 0.1% for 20 iterations.

3. Results

Parallel simulations of chair rise and gait required 60 h using a desktop workstation with 16 Intel® Xeon® 3.50 GHz processors and 64.0 GB of memory. Each iteration of static optimization took approximately 6 min of computational time requiring a maximum of 600 iterations to complete all 13 timepoints. Results reported for both models are ordered as Model 1 (“M1”) and Model 2 (“M2”), unless otherwise stated.

Predicted activations during chair rise matched normalized subject EMG in both trend and magnitude (Fig. 2) with no notable differences between models M1 and M2. Muscle forces for the quadriceps, echoing the model activations and subject EMG, peaked at the beginning of the chair rise (2174 N, 1962 N) and decreased throughout the activity (Fig. 3). The gluteus maximus exhibited a similar trend with large forces (1278 N, 1109 N) at the beginning that decreased throughout the activity. Iliopsoas

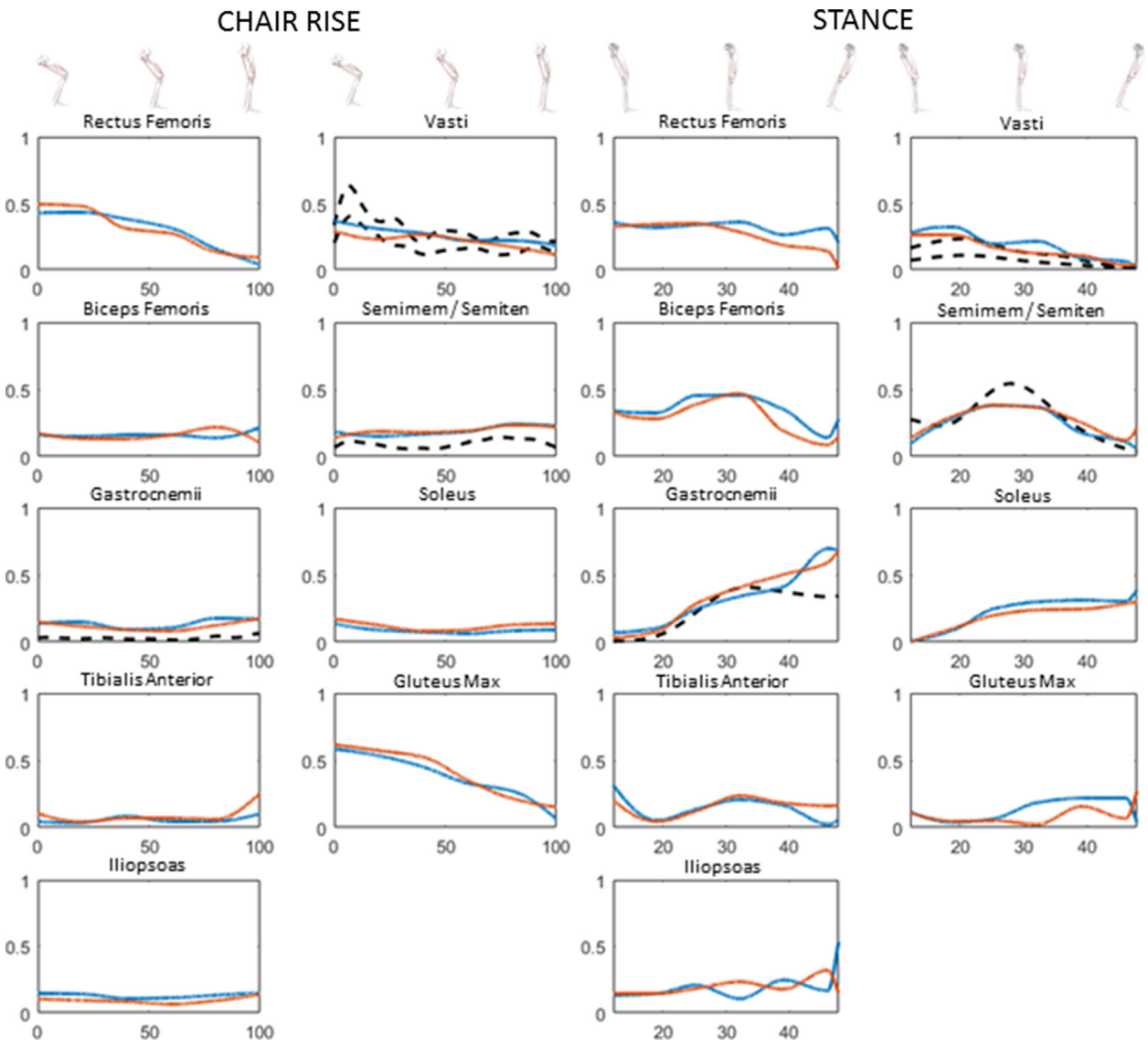

Fig. 2. Predicted model activations for Model 1 (red) and Model 2 (blue) and normalized subject EMG (black dashed) plotted for chair rise (left) and the stance phase of gait (right). (For interpretation of the references to color in this figure legend, the reader is referred to the web version of this article.)

and hamstrings produced little force during the activity. Gastrocnemii and soleus forces were largest at the beginning (828 N, 919 N) and end (657 N, 799 N) of the chair rise. Normalized subject EMG recorded from the medial gastrocnemius started at 4% activation and increased toward full extension. However, the estimated activation fell between 5% and 20% activation but was similar in trend for both M1 and M2.

During the chair rise activity, total TF contact forces (calculated along the superior-inferior axis of the tibia) peaked early in the activity (337%BW, 341%BW) and then decreased as the subject progressed to stance (Fig. 3). PF contact forces echoed the estimated quadriceps forces and peaked at the beginning of chair rise (227% BW, 233%BW) and decreased with knee flexion angle. PCL, MCL, and PFL force peaked at the beginning of the chair rise (413 N, 425 N, and 368 N (M1), and 575 N, 327 N, and 225 N (M2), respectively), and diminished as knee flexion decreased.

During the gait activity, quadriceps forces peaked during contralateral toe off (CTO) (896 N, 870 N) and decreased through stance phase to contralateral heel strike (CHS) (Fig. 4). Normalized subject EMG peaked at 35% and 33% of stance for the medial and lateral vasti, respectively. Maximum hamstring forces occurred midway through single limb support (851 N, 868 N) and decreased through stance to CHS. Normalized subject EMG peaked for medial hamstrings at 46% of stance. Predicted activations for hamstrings matched normalized subject EMG with peaks occurring at 54% of stance for both models. Gastrocnemii and soleus force was small at CTO (181 N, 90 N), echoed by predicted model activations and subject EMG, then increased throughout stance peaking at CHS (2171 N, 2281 N). Muscle forces from iliopsoas increased during stance with M1 forces ultimately increasing (520 N) at CHS and M2 forces decreasing at CHS (234 N).

During the stance phase of gait, total TF contact forces increased throughout stance until CHS (402%BW, 397%BW) (Fig. 4). Both M1 and M2 started with a 50%/50% medial to lateral distribution of contact at CTO and deviated throughout the trial to 79%/21% and 89%/11% at CHS for the two models, respectively. The patella was in contact with the femur from CTO to mid-stance with maximum contact occurring at CTO (36%BW, 25%BW). The ACL, PCL, and MCL carried load during the second half of stance, with respective peaks of 293 N, 122 N, and 120 N (M1) and 213 N, 81 N, and 163 N (M2).

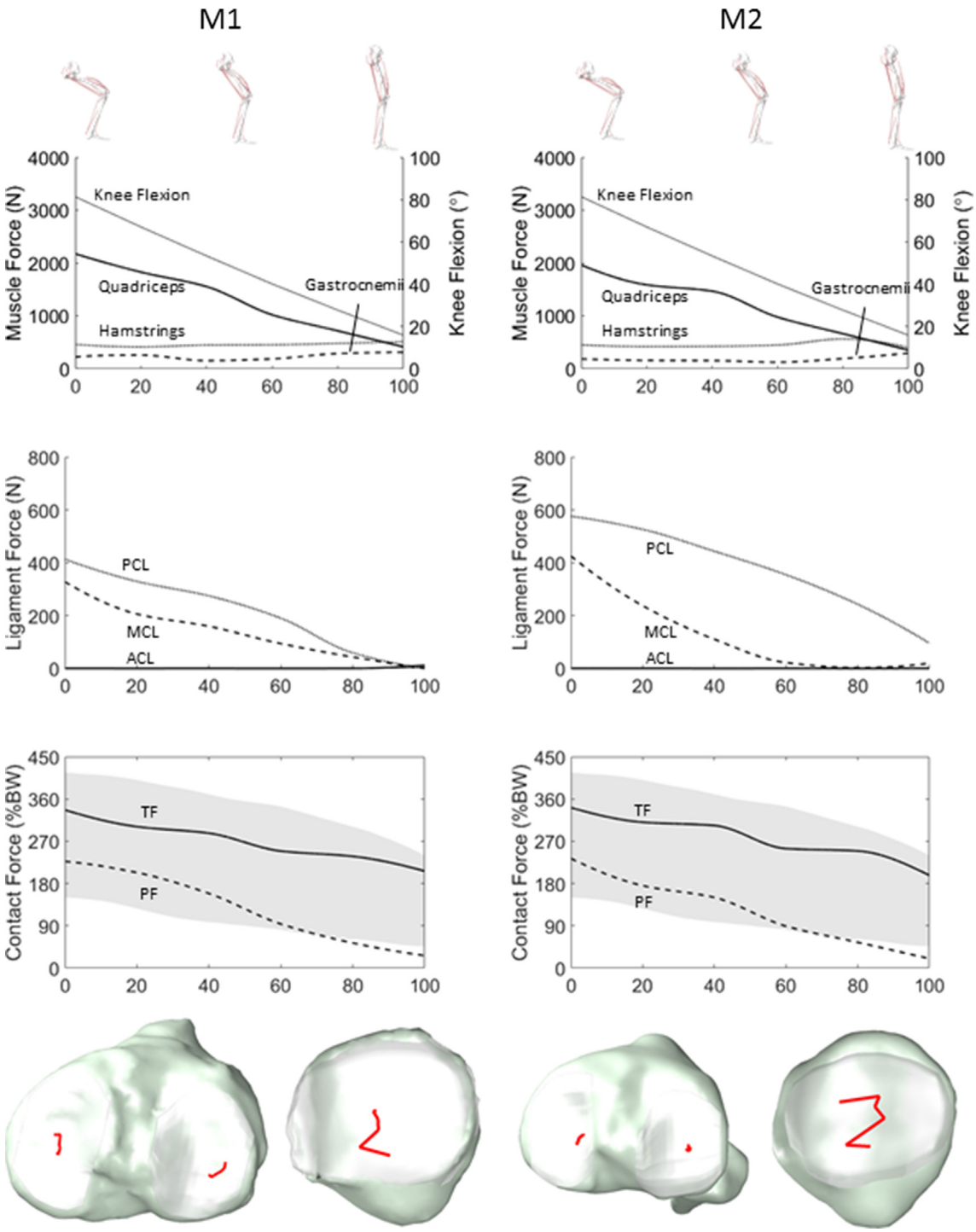

Fig. 3. Forces prescribed by static optimization in muscles groups crossing the knee, forces carried by tibiofemoral ligaments, contact forces (TF/PF) plotted against telemetric implant data (Bergmann et al., 2014), and motion of COP during the chair rise activity.

4. Discussion

A multi-scale musculoskeletal model of the lower extremity that combined muscle modeling and FE analysis was created and used in a static optimization to simultaneously solve for muscle forces and TF and PF mechanics during a chair rise and the stance phase of gait. The musculoskeletal model combined representations of the bones, muscles, tendons, and ligaments into a single model of the lower extremity. Two separate knee models with calibrated specimen-specific ligament representations were used to illuminate differences due to geometry and soft tissue calibration. The results showed that muscle forces can be calculated in a single framework without the use of serial rigid-body and FE models with inherently dissimilar geometry, loading conditions, and scales. Our solution was important because it demonstrated that a detailed representation of muscle geometry and properties can be combined with specimen-specific representation of the bone and soft tissues of the knee to predict muscle forces, and soft tissue and joint mechanics simultaneously.

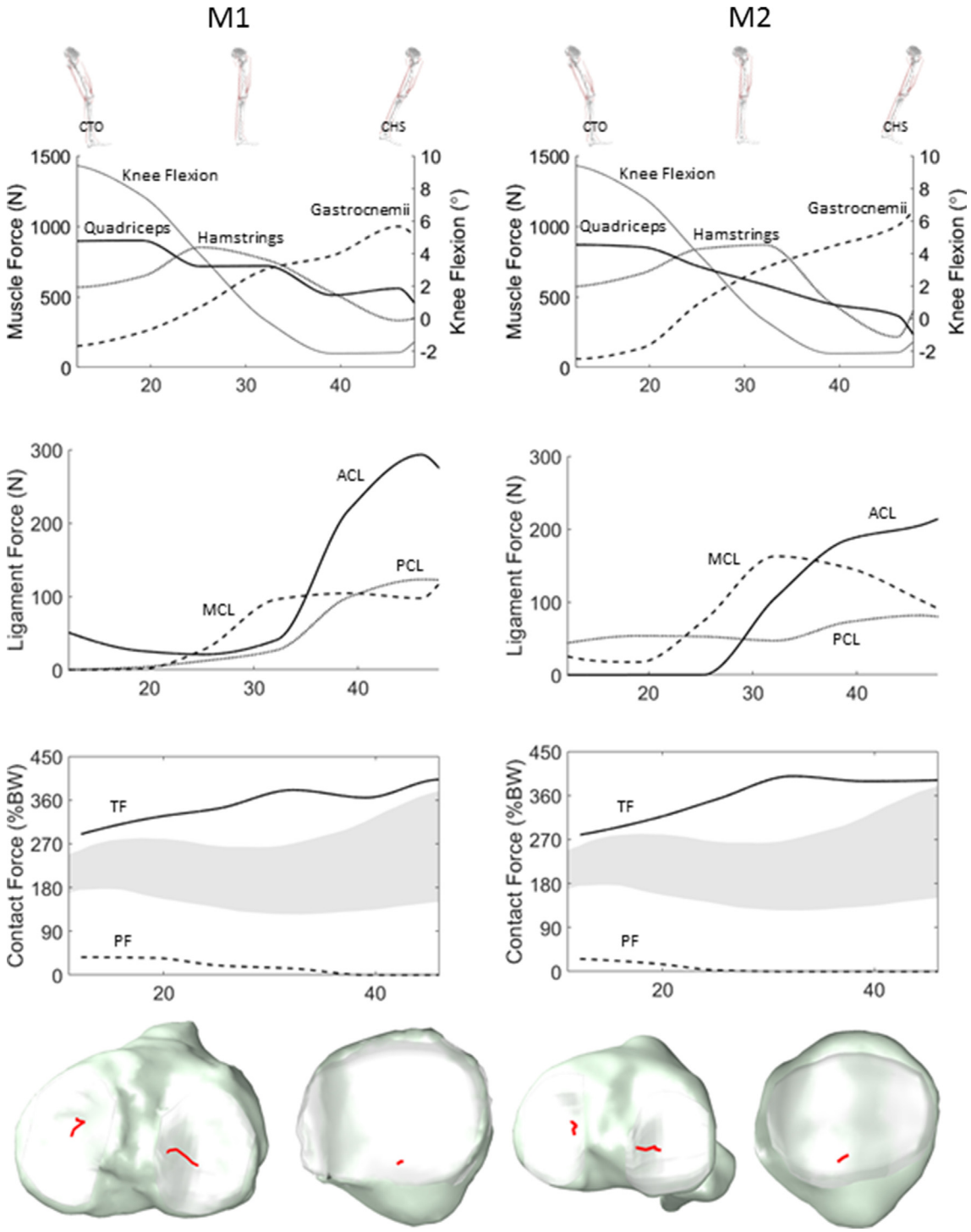

Fig. 4. Forces prescribed by static optimization in muscles groups crossing the knee, forces carried by tibiofemoral ligaments, contact forces (TF/PF) plotted against telemetric implant data (Bergmann et al., 2014), and motion of COP during the gait activity.

Required computational time for the present study was shorter than recent FE optimization-based solutions, which reported computational times between 32 h and 4 weeks (Halloran et al., 2010, 2009; Lin et al., 2010), and often include planar models of the joints (Halloran et al., 2010, 2009) and surrogate representations of the contact mechanism (Halloran et al., 2009; Lin et al., 2010). While rigid body dynamics simulations allow for fast convergence of static optimization solutions (Smith et al., 2015; Thelen et al., 2014) and forward dynamics solutions (Guess et al., 2014), they are limited in their ability to model complex anisotropic material representations (Ali et al., 2017). The work presented here demonstrated three-dimensional analysis of tissue strains of individuals performing dynamic activities in a finite element framework using optimization-based muscle prediction.

Muscle forces predicted during the chair rise activity were similar in trend and magnitude to previous predictions. Shelburne and Pandy (2002) reported peak quadriceps forces at 80° of knee flexion of 2800 N compared to 2174/1962 N, for M1 and M2, respectively. Predicted hamstrings forces were nearly identical to those presented in this study with peak forces of 500 N throughout the

activity. Although the subject from the present study was slightly heavier, Shelburne and Pandy (2002) instructed their subject to rise "as quickly as possible" which might explain the discrepancy in quadriceps muscle forces. Joint loads predicted by the simulation were like previous joint load predictions and measurements made using telemetric implants. Peak tibiofemoral and patellofemoral contact forces were seen at 0% cycle: 336/341%BW and 227/233%BW respectively. Our results for TF contact fall within ±2σ bounds representative of 7 subjects with telemetric implants performing a chair rise (Bergmann et al., 2014). Shelburne and Pandy (2002) reported similar results for TF contact, but with larger magnitude of PF contact at 80° knee flexion, 450%BWs compared to 227/233%BW. Contact forces in both PF and TF decreased through the activity, as expected based on decreasing quadriceps muscle forces. Ligament forces predicted by the models were similar with previously published work. During the chair rise task, the PCL carried most of the shear load, with peak force of 413/575 N occurring at 80° of knee flexion. Shelburne and Pandy (2002) reported larger peak PCL force (650 N), with minimal MCL contribution (max: 50 N) and negligible ACL contribution. Our work indicated load sharing between the PCL and MCL (max: 327 N, 425 N) in deep flexion. This is likely explained by the internal-external DOF represented in the present model, compared to the planar representation from Shelburne and Pandy (2002).

Muscle forces compared well with previous predictions performed using static optimization during instrumented (Lin et al., 2010) and healthy gait (Adouni and Shirazi-Adl, 2014b; Anderson and Pandy, 2001b). Previously reported peak vasti forces fell between 600 and 1200 N compared to 510/525 N at CTO, and peak gastrocnemii forces between 300 and 900 N compared to 1000/1112 N at CHS. Previous results predicted 300 N (Anderson and Pandy, 2001b), between 0 and 600 N (Lin et al., 2010), and 225 N (Adouni and Shirazi-Adl, 2014b) of hamstring force, where our models predicted peak hamstring forces 851/868 N during mid stance (30% cycle), following the shape of normalized subject EMG. Models moderately overpredicted TF contact forces when compared to ±2σ bounds representative of 6 subjects with telemetric implants during gait with 381/396%BW TF contact at CHS. The expected two-peak shape of the TF contact loading was not evident, likely attributed by the uncharacteristically large hamstrings loads predicted by the simulations. The patella remained in contact until midstance, which can be explained by the hyper extension of the knee measured with stereo radiography. ACL forces were greater in gait than chair rise, with peak magnitudes occurring at CHS (293,205 N). Similar trends can be found in previous work, which showed increasing ACL loading profile as the knee was hyperextended, with a mean of 80 N in 2° of hyperextension (Jagodzinski et al., 2003).

The differences in the optimization results from the two knee models demonstrated the importance of calculating muscle forces and joint mechanics simultaneously (Fiorentino, 2013; Hume et al., 2018; Lunnen et al., 1981; Navacchia et al., 2017). The two knee models produced results which were similar in trend, but with different load sharing of the functional muscle groups. Specifically, the peak quadriceps force output was 11% larger during the chair rise task for M1. Furthermore, the movement of the COP on the patellar cartilage (Fig. 3) illustrated differences in load sharing between the vastus medialis and vastus lateralis. At 0% cycle the %VM/%VL to total quadriceps force was 51%/21% and 60%/13% for the two models, respectively. This ratio of contribution changed throughout the activity concluding at 100% cycle with 38%/33% and 35%/40%. The change in contribution of different muscles at varying normalized fiber lengths highlighted the ability of static optimization to resolve the muscle redundancy problem effectively and the sensitivity of muscle forces to variation in articular geometry (Smoger et al., 2015), ligament representation (Smith et al., 2015), and muscle moment arms that occurs in a deforming model of the joint (Hume et al., 2018). This sensitivity further highlights the importance of an approach which includes muscle force estimation with soft tissue modeling in a single framework.

The present study included several limitations. First, the kinematics and kinetics applied to the models came from an *in vivo* study whereas the geometry and calibration of the knee models were derived from *in vitro* measurements of cadaveric specimens. Secondly, predictions of joint forces during most activities depend heavily on the muscle forces calculated for the activities (Shelburne et al., 2006). While no data exist to directly confirm the calculated values of the muscle forces obtained here for squatting, the predicted joint loads, and muscle activation patterns compared favorably with measurements of the same activities obtained *in vivo*. For example, the level of vastus activation and muscle force decreased as the subject moved through stance, while gastrocnemius muscle force increased through CHS (Fig. 4). In addition, joint loads during chair rise were like those obtained using telemetric tibial implants. To better understand the uncertainty in model inputs and outputs, this work could benefit from a deterministic analysis that considers how variation in musculotendon parameters (Navacchia et al., 2016a), modeling uncertainty (Myers et al., 2015), and geometric variation (Easley et al., 2007) affect model response. A final limitation was that the optimization took 60 h of computational time on 13 cores for each subject. However, the current FE framework has the advantage of allowing modular complexity in tissue definitions that can dramatically affect, increase or decrease, solution speeds. This capability allows solution refinement, by increasing the number and complexity of deformable tissues, as the simulation progresses. In addition, ever increasing numbers of processers and processer speeds will further enable practical use of deformable, multi-scale musculoskeletal simulations.

In summary, a detailed multi-scale MSFE model with calibrated soft tissue response was used to perform simultaneous predictions of muscle forces, joint mechanics, and loading of structures using laboratory data from subjects as input. This study demonstrates the feasibility of predicting muscle forces in dynamic, muscle-driven simulations that maintain high-fidelity deformable joint representations. This methodology can be used in clinically relevant evaluation of the interplay between muscle, ligament, and cartilage that occur due to injury, pathology, or surgical intervention at the joint level scale and muscle mechanics and function at the whole-body scale.

Acknowledgements

Supported by a grant from the NIH National Institute of Biomedical Imaging and Bioengineering (R01EB015497).

References

Adouni, M., Shirazi-Adl, A., 2014a. Evaluation of knee joint muscle forces and tissue stresses-strains during gait in severe OA versus normal subjects. J. Orthop. Res. 32, 69–78.

Adouni, M., Shirazi-Adl, A., 2014b. Partitioning of knee joint internal forces in gait is dictated by the knee adduction angle and not by the knee adduction moment. J. Biomech. 47, 1696–1703.

Adouni, M., Shirazi-Adl, A., Shirazi, R., 2012. Computational biodynamics of human knee joint in gait: from muscle forces to cartilage stresses. J. Biomech. 45, 2149–2156.

Ali, A.A., Harris, M.D., Shalhoub, S., Maletsky, L.P., Rullkoetter, P.J., Shelburne, K.B., 2017. Combined measurement and modeling of specimen-specific knee mechanics for healthy and ACL-deficient conditions. J. Biomech. 57, 117–124.

Ali, A.A., Shalhoub, S.S., Cyr, A.J., Fitzpatrick, C.K., Maletsky, L.P., Rullkoetter, P.J., Shelburne, K.B., 2016. Validation of predicted patellofemoral mechanics in a finite element model of the healthy and cruciate-deficient knee. J. Biomech. 49, 302–309.

Anderson, F., Pandy, M., 2001a. Dynamic optimization of human walking. J. Biomech. Eng. 123, 381.

Anderson, F., Pandy, M., 2001b. Static and dynamic optimization solutions for gait are practically equivalent. J. Biomech. 34, 153–161.
Anderson, F.C., Pandy, M.G., 2003. Individual muscle contributions to support in normal walking. Gait Posture 17, 159–169.
Arnold, E.M., Delp, S.L., 2011. Fibre operating lengths of human lower limb muscles during walking. Philos. Trans. R. Soc. Lond. B. Biol. Sci. 366, 1530–1539.
Baldwin, M., Clary, C., Maletsky, L.P., Rullkoetter, P.J., 2009. Verification of predicted specimen-specific natural and implanted patellofemoral kinematics during simulated deep knee bend. J. Biomech. 42, 2341–2348.
Bergmann, G., Bender, A., Graichen, F., Dymke, J., Rohlmann, A., Trepczynski, A., Heller, M.O., Kutzner, I., 2014. Standardized loads acting in knee implants. PLoS One 9, e86035.
Besier, T.F., Fredericson, M., Gold, G.E., Beaupré, G.S., Delp, S.L., 2009. Knee muscle forces during walking and running in patellofemoral pain patients and pain-free controls. J. Biomech. 42, 898–905.
Buford, W., Ivey, F.M.J., Malone, J.D., Patterson, R.M., Peare, G.L., Nguyen, D.K., Stewart, A.A., 1997. Muscle balance at the knee – moment arms for the normal knee and the ACL-minus knee. IEEE Trans. Rehabil. Eng. 5, 367–379.
Crowninshield, R.D., Brand, R.A., 1981. A physiologically based criterion of muscle force prediction in locomotion. J. Biomech. 14, 793–801.
Delp, S.L., Anderson, F.C., Arnold, A.S., Loan, P., Habib, A., John, C.T., Guendelman, E., Thelen, D.G., 2007. OpenSim: open-source software to create and analyze dynamic simulations of movement. IEEE Trans. Biomed. Eng. 54, 1940–1950.
Easley, S.K., Pal, S., Tomaszewski, P.R., Petrella, A.J., Rullkoetter, P.J., Laz, P.J., 2007. Finite element-based probabilistic analysis tool for orthopaedic applications. Comput. Methods Programs Biomed. 85, 32–40.
Fernandez, J.W., Hunter, P.J., 2005. An anatomically based patient-specific finite element model of patella articulation: towards a diagnostic tool. Biomech. Model. Mechanobiol. 4, 20–38.
Fiorentino, N.M., 2013. Rectus femoris knee muscle moment arms measured in vivo during dynamic motion with real-time magnetic resonance imaging. J. Biomech. Eng. 135, 044501.
Fitzpatrick, C.K., Baldwin, M.A., Rullkoetter, P.J., 2010. Computationally efficient finite element evaluation of natural patellofemoral mechanics. J. Biomech. Eng. 132, 121013.
Guess, T.M., Stylianou, A.P., Kia, M., 2014. Concurrent prediction of muscle and tibiofemoral contact forces during treadmill gait. J. Biomech. Eng. 136, 021032.
Halloran, J.P., Ackermann, M., Erdemir, A., van den Bogert, A.J., 2010. Concurrent musculoskeletal dynamics and finite element analysis predicts altered gait patterns to reduce foot tissue loading. J. Biomech. 43, 2810–2815.
Halloran, J.P., Erdemir, A., van den Bogert, A.J., 2009. Adaptive surrogate modeling for efficient coupling of musculoskeletal control and tissue deformation models. J. Biomech. Eng. 131, 011014.
Harris, M.D., Cyr, A.J., Ali, A.A., Fitzpatrick, C.K., Rullkoetter, P.J., Maletsky, L.P., Shelburne, K.B., 2016. A combined experimental and computational approach to subject-specific analysis of knee joint laxity. J. Biomech. Eng. 138, 081004.
Hume, D.R., Navacchia, A., Ali, A.A., Shelburne, K.B., 2018. The interaction of muscle moment arm, knee laxity, and torque in a multi-scale musculoskeletal model of the lower limb. J. Biomech. 76, 173–180.
Jagodzinski, M., Leis, A., Iselborn, K.W., Mall, G., Nerlich, M., Bosch, U., 2003. Impingement pressure and tension forces of the anterior cruciate ligament. Knee Surgery Sport. Traumatol. Arthrosc. 11, 85–90.
Kefala, V., Cyr, A.J., Harris, M.D., Hume, D.R., Davidson, B.S., Kim, R.H., Shelburne, K. B., 2017. Assessment of knee kinematics in older adults using high-speed stereo radiography. Med. Sci. Sports Exerc. 49, 2260–2267.
Lenhart, R.L., Kaiser, J., Smith, C.R., Thelen, D.G., 2015. Prediction and validation of load-dependent behavior of the tibiofemoral and patellofemoral joints during movement. Ann. Biomed. Eng. 43, 2675–2685.
Lin, Y.-C., Walter, J.P., Banks, S.A., Pandy, M.G., Fregly, B.J., 2010. Simultaneous prediction of muscle and contact forces in the knee during gait. J. Biomech. 43, 945–952.
Lunnen, J.D., Yack, J., LeVeau, B.F., 1981. Relationship between muscle length, muscle activity, and torque of the hamstring muscles. Phys. Ther. 61, 190–195.
Myers, C.A., Laz, P.J., Shelburne, K.B., Davidson, B.S., 2015. A probabilistic approach to quantify the impact of uncertainty propagation in musculoskeletal simulations. Ann. Biomed. Eng. 43, 1098–1111.
Navacchia, A., Kefala, V., Shelburne, K.B., 2017. Dependence of muscle moment arms on in vivo three-dimensional kinematics of the knee. Ann. Biomed. Eng. 45, 789–798.
Navacchia, A., Myers, C.A., Rullkoetter, P.J., Shelburne, K.B., 2016a. Prediction of in vivo knee joint loads using a global probabilistic analysis. J. Biomech. Eng. 138, 031002.
Navacchia, A., Rullkoetter, P.J., Schütz, P., List, R.B., Fitzpatrick, C.K., Shelburne, K.B., 2016b. Subject-specific modeling of muscle force and knee contact in total knee arthroplasty. J. Orthop. Res. 34, 1576–1587.
Shelburne, K.B., Pandy, M.G., 2002. A dynamic model of the knee and lower limb for simulating rising movements. Comput. Methods Biomech. Biomed. Eng. 5, 149–159.
Shelburne, K.B., Torry, M.R., Pandy, M.G., 2005. Muscle, ligament, and joint-contact forces at the knee during walking. Med. Sci. Sports Exerc. 37, 1948–1956.
Shelburne, K.B., Torry, M.R., Pandy, M.G., 2006. Contributions of muscles, ligaments, and the ground-reaction force to tibiofemoral joint loading during normal gait, 1983–1990.
Smith, C., Lenhart, R., Kaiser, J., Vignos, M., Thelen, D., 2015. Influence of ligament properties on tibiofemoral mechanics in walking. J. Knee Surg. 29, 099–106.
Smoger, L.M., Fitzpatrick, C.K., Clary, C.W., Cyr, A.J., Maletsky, L.P., Rullkoetter, P.J., Laz, P.J., 2015. Statistical modeling to characterize relationships between knee anatomy and kinematics. J. Orthop. Res. 33, 1620–1630.
Thelen, D.G., Won Choi, K., Schmitz, A.M., 2014. Co-simulation of neuromuscular dynamics and knee mechanics during human walking. J. Biomech. Eng. 136, 021033.
Walter, J.P., Korkmaz, N., Fregley, B., Pandy, M., 2015. Contribution of tibiofemoral joint contact to net loads at the knee in gait. J. Orthop. Res., 33